



OPEN

Particle size effect on sorting with optical lattice

Ebrahim Madadi¹, Morad Biagooni², Farhad Mohammadjafari³ & SeyedEhsan Nedaaee Oskoei^{2,4}✉

Transport of mesoscale particles due to driving flow fields or external forces on a periodic surface appears in many areas. Geometrical and physical characteristics of particles affect the velocities of the particles in these periodic landscapes. In this paper, we present a numerical simulation based on solving the Langevin equation for the meso-size particles subjected to the thermal fluctuations in a periodic array of optical traps. We consider the real-size particles which cause the partial trapping of particles in the optical traps. The particles are sorted for the size-dependency of particles' trajectories. Our results are in good agreement with experiments.

Sorting of the mesoscale particles on a periodic two-dimensional energy landscape is of great current interest, both theoretically and experimentally. Holographic optical tweezers (HOT) are the common technique to generate such energy landscapes. Examples include the study of the transport of colloidal particles through arrays of micro-scale potential landscapes in the HOT generated potential wells¹⁻⁶, investigation of transport and separation of overdamped particles in a microfluidic system⁷, sorting of chiral particles exploiting lattice potentials⁸, dynamic ordering and locking states of colloidal monolayers on a decagonal quasiperiodic surface⁹, sortings of particles within a microfluidic chip using a dual-channel line optical tweezers with a 'Y' shape channel¹⁰ and, experimental investigation for the transport of 100 and 500 nm plasmonic nanoparticles in a two-dimensional optical lattice¹¹. An array of obstacles on a surface is another technique for separating mesoscale particles¹²⁻²³. In both cases, sorting occurs based on the fact that because of the potential wells (obstacles), particles' path deviates from the direction of the external force (fluid flow). This deviation depends on many parameters including the strength of the potential wells (obstacles), size of the wells, external force, particle dielectric constant, shape, and size of the particles. The deviation angle in a single experimental setup depends on the characteristic properties of the particle, mostly their shapes, and sizes.

As a common method of generating HOTs, a diffractive beam splitter usually converts a single laser beam to several beams, each of which forms an individual optical trap²⁴. A computer-generated hologram usually employs such a beam splitter to generate multiple traps. An array of optical tweezers can be generated in any dimension and any configuration, by making use of this method. For instance, one can refer to prismatic optical fractionation studied recently by Xiao et al.⁶. They showed that simultaneous and continuous sorting of heterogeneous samples into multiple spatially separated fractions can be done using an especial arrangement of optical traps. In addition to the collective properties of optical wells (traps), specific properties of a single well such as its width and depth can be controlled in this method. All of the above-mentioned advantages of the HOT method provide an easy fabricating device to sort an especial kind of particle.

Another method for sorting of micro-scale particles is an array of micro-scale size obstacles in the path of laminar flow of suspended particles using microfabrication techniques. As an example of such a microfabricated device, one can refer to the work by Huang et al.¹², in which a two-dimensional matrix of silicon obstacles was employed for the separation of flexible biological molecules such as DNA without jamming or clogging. In this work, successive rows were slightly shifted laterally, which cause the fluid bifurcates flowing through the obstacles. This bifurcation of the laminar flow is asymmetric, and cause different path for particles of different size which are passing through the obstacles array. Many different papers in the literature have been devoted to the separation of particles by making use of locking states which occur on periodic surfaces. For instance, directional locking of particles in a fluid-driven through a regular lattice of cylindrical obstacles¹³, separation of drops¹⁴, the effects of the particle deformability on the separation of particles¹⁷, directional lockings in microfluidic separation systems¹⁸, clogging and jamming transitions for bidisperse disks flowing through a two-dimensional periodic

¹Department of Engineering Sciences and Physics, Buein Zahra Technical University, Buein Zahra, Qazvin, Iran. ²Department of Physics, Institute for Advanced Studies in Basic Sciences (IASBS), GavaZang, Zanjan 45137-66731, Iran. ³Payame Noor University, Nakhl St., Artesh Blvd., Minicity, Tehran 19395-4697, Iran. ⁴Research Center for Basic Sciences & Modern Technologies (RBST), Institute for Advanced Studies in Basic Sciences (IASBS), GavaZang, Zanjan 45137-66731, Iran. ✉email: nedaaee@iasbs.ac.ir

obstacle array²⁵, locking modes of the superparamagnetic beads transported in a 2D potential landscape²⁶ have been studied.

Despite sorting of particles on a periodic potential landscape which is produced by HOTs, locking states have been observed in other physical phenomena. For instance, separation of particles and cells by making use of an array of slanted open cavities¹⁶, locking phases for the skyrmion motion on a periodic substrate²⁷, phase-locking for vortex lattices on a superconducting periodic pinning array²⁸, directional lockings of vortices and colloids over a square and triangular periodic substrate²⁹, directional lockings of a monolayer of paramagnetic particles across a periodic substrate of a triangular lattice of magnetic bubbles³⁰, have been investigated.

Many parameters affect the efficiency of sorting, including the physical properties of individual particles such as their shape and size, stiffness, and optical properties as well as their collective properties like particle density. Furthermore, the external force (laminar flow velocity), the density of traps (obstacles), and their configuration play an important role in the particle separation. The temperature plays an important role in sorting by arrays of potential wells. This is because in the case of potential wells, escaping of a trapped particle depends on the thermal fluctuations of the particle in the trap.

Since the number of parameters in the sorting process is relatively large, experimental studies can not cover all details of such a complex phenomenon, and therefore, some theoretical attempt is needed. As a preliminary effort to the theoretical study of this phenomenon, Lacasta et al. did some simulations on the classical particles sorting in a periodic potential landscape that was created by two-dimensional traps of optical tweezers³¹. They used a point-like classical particle in their simulations. The use of point-like particles causes discrepancy with the experimental results. To overcome the discrepancy with experimental results, more details are needed to take into account in the simulations. In our work, instead of considering point-like particles and modeling the size of a real particle with the width of the potential wells, we modeled the particle using a combination of point-like particles on a circumference of a circle. This can be considered as a simplified model for a spherical particle in a two-dimensional space, which our simulations were carried out. We have shown that in this case, the “*partial trapping*” phenomenon plays an important role in the sorting of particles of different sizes. The term *partial trapping* comes from the fact that only a portion of the particle may be affected by the potential well and as a result, the traveling particle does not trap by the well completely, however, its trajectory deflects from the original path. We have shown that partial trapping causes a notable decrease in the size of the middle plateau and make a better agreement with the experimental data.

Methods

Lacasta et al.³¹, modeled the sorting of the particles on an array of periodic potential wells landscape. They considered a classical particle which is driven by an external force through an array of optical traps which were generated by a two-dimensional periodic function. The particle which they used in their simulations was a point-like classical particle, therefore in order to model the size of particles, they changed the width of traps. In this scenario, particles of small size were modeled by wider wells and on the contrary, narrow wells were used to model those of larger size. The governing equation of motion of the point-like particles were the Langevin equation, which includes a random force to mimic the effect of thermal fluctuations. Their results contained plateaus in the plot of absolute velocity angle for the external force angle, which belongs to the “kinetically locked-in states”. These plateaus were reported in experimental papers as well. (see, for example, Fig. 5 of Ref.¹ and Fig. 2 of Ref.⁹) However, there is a middle large plateau in simulation results which its experimental correspondence is not nearly as large as simulation^{1,9}. This incongruity was removed by increasing the temperature in Lacasta’s simulations, however, small kinetically locked-in plateaus were disappeared too, in contradiction with experiment. This discrepancy between simulation and experimental outputs can be a result of the dimensionless point-like particles which have been used in numerical simulations.

A point-like particle has two states when passing through the vicinity of a trap: (i) it is fully trapped by the potential well, and (ii) passing it without feeling any force. This, however, is in contrast with what usually happens in the real case, in which in addition to two above states, a particle can be partially trapped in the potential well as it is schematically illustrated in Fig. 1a. In the latter, a portion of the particle intersects with the boundary of the potential well, and as a result, depending on the size of this portion, the particle may pass the well without trapping by it. Nonetheless, the particle’s direction of motion slightly changes because the applied force from the trap, in comparison with the drag force, is not strong enough to pull the particle inside and just makes a small deviation in the particle’s trajectory.

To model the partial trapping effect, we model the suspended particle by a combination of point-like particles that are connected with elastic bands and form a quasi-sphere, as it is shown schematically in Fig. 1b. Elastic connectors obey the Hook’s law:

$$U(r_{ij}) = \frac{1}{2}K(r_{ij} - r_0)^2, \quad (1)$$

in which $r_{ij} = |\mathbf{r}_i - \mathbf{r}_j|$ is the relative distance between the adjacent mass of a particle, r_0 is the equilibrium distance between connected particles and K is the spring stiffness constant. To let the particle to be flexible, we considered a bending potential between adjacent pair of particles:

$$U(\gamma) = \frac{1}{2}K_\gamma(\gamma - \gamma_0)^2, \quad (2)$$

where K_γ is the *bending stiffness constant* and γ_0 is the *equilibrium angle* between adjacent pair of particles which its numeric value depends on the initial form of the combination. In order to take the flow effect into account, each constructing particle is subjected to an external force $\mathbf{f}_i = f_0(\cos \theta_i \hat{\mathbf{x}} + \sin \theta_i \hat{\mathbf{y}})$ of a constant modulus f_0 ,

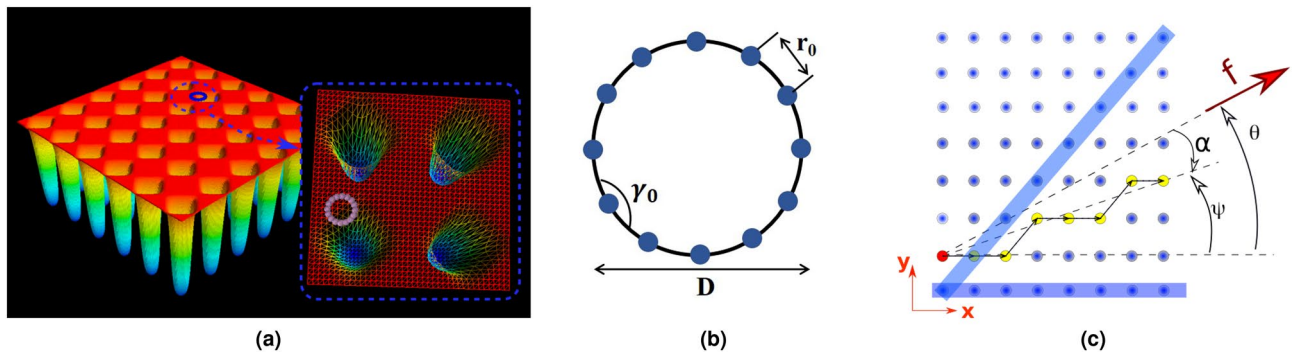


Figure 1. (a) Schematics illustration for partial trapping. As it is clear from this figure, only a small part of the particle feels potential well. This part of the figure is drawn with Mayavi³². (b) A combination of 12 point-like particles are placed together on the circumference, connected via springs to form a quasi-sphere. (c) Schematic representation of simulation setup. Blue strips are potential channels, as is explained in the text. (.)

which makes an angle θ_i with the direction x of the 2-D array of potential wells in the Cartesian coordinate system. As the original potential form used by Lacasta³¹, we modeled the two-dimensional array of potential wells by using a periodic function of characteristic length scale λ :

$$V(x, y) = \frac{V_0}{1 + e^{-g(x,y)}}, \tag{3}$$

in which V_0 is a measure of the depth of well and $g(x, y) = A[\cos(2\pi x/\lambda) + \cos(2\pi y/\lambda) - 2B]$ is a periodic function of coordinate. Parameters A and B control the steepness of the potential wells and their relative size with respect to the spatial period λ .

We used the standard Langevin molecular dynamics method to simulate the transport of individual particles. At each stage of simulation, only one particle passes through the array of traps. The governing equation of motion for each particle is as follow:

$$m\ddot{\mathbf{r}}_i = -\nabla_i U - \mu\dot{\mathbf{r}}_i + \mathbf{f}_i + \xi_i(t), \tag{4}$$

where $U = U(r_{i,j}) + U(\gamma) + V(x, y)$ is the summation of individual potentials, the subscript i indicates the point-like constructing particles and μ is the phenomenological coefficient of the drag force. $\xi_i(t)$ is the mutually uncorrelated thermal force acting on each particle obeying the fluctuation-dissipation relation;

$$\langle \xi_{i,\alpha}(t)\xi_{j,\beta}(t') \rangle = 2\mu k_B T \delta_{ij} \delta_{\alpha\beta} \delta(t - t'), \tag{5}$$

where the subscripts α and β denote different components of the random forces, i and j indicate the individual constructing particles and k_B is the Boltzmann constant.

We used the scaled variables, $\tilde{\mathbf{r}} = \mathbf{r}/\lambda$, $\tilde{t} = t\sqrt{V_0/(m\lambda^2)}$ to make the Eq. (4) dimensionless. This reduces the number of independent variables and makes it easier to study the model. The remaining independent variables are as follow:

$$\begin{aligned} \tilde{T} &= T \frac{k_B}{V_0}, \quad \tilde{\mu} = \mu \frac{\lambda}{\sqrt{mV_0}}, \quad \tilde{f}_0 = f_0 \frac{\lambda}{V_0}, \\ \tilde{K} &= K \frac{\lambda^2}{V_0^2}, \quad \tilde{K}_\theta = K_\theta \frac{\lambda^2}{V_0}, \quad \tilde{\mathbf{r}}_0 = \mathbf{r}_0 \frac{1}{\lambda}. \end{aligned} \tag{6}$$

Therefore, the dimensionless equation of motion is

$$\ddot{\mathbf{r}}_i = -\nabla_i U - \mu\dot{\mathbf{r}}_i + \mathbf{f}_i + \zeta_i(t), \tag{7}$$

in which we removed the tilde signs of all variables and parameters in the rest of the paper for convenience. $\zeta_i(t)$ is the dimensionless thermal force which obeys the following fluctuation-dissipation relation;

$$\langle \zeta_{i,\alpha}(t)\zeta_{j,\beta}(t') \rangle = 2\mu T \delta_{ij} \delta_{\alpha\beta} \delta(t - t'). \tag{8}$$

The resulting set of coupled *stochastic ordinary differential equations* (SODE) was solved using the *second-order stochastic Runge-Kutta* (SRKII) algorithm³³. We used the Box-Muller transformation³⁴ to generate the random variables with Gaussian distribution. Results are averaged over 1000 independent initial conditions and the integration was performed for 10^5 time steps with dimensionless time step increment $\Delta t = 0.005$. As the original work by Lacasta, we set the numeric values of parameters $A = 5$, $\lambda = 1$, $f_0 = 8$ and $\mu = 20$, which did not change during the simulation. We chose the K and K_γ in such a way that the particle behaves like a rigid one. r_0 and γ_0 could be calculated by making use of the particle's diameter.

In this work, we studied deviation in the direction of the velocity of the center of mass of particles from the direction of the applied force (external flow), as a function of B and T . The Cartesian components of the average velocity were evaluated in the similar method as reference³¹. $\langle v_\beta \rangle = \lim_{t \rightarrow \infty} \langle r_\beta(t) \rangle / t$, where $\beta = x, y$ and $\langle \cdot \rangle$ means average of all distinct configurations. In addition to the Cartesian components of the particles velocity,

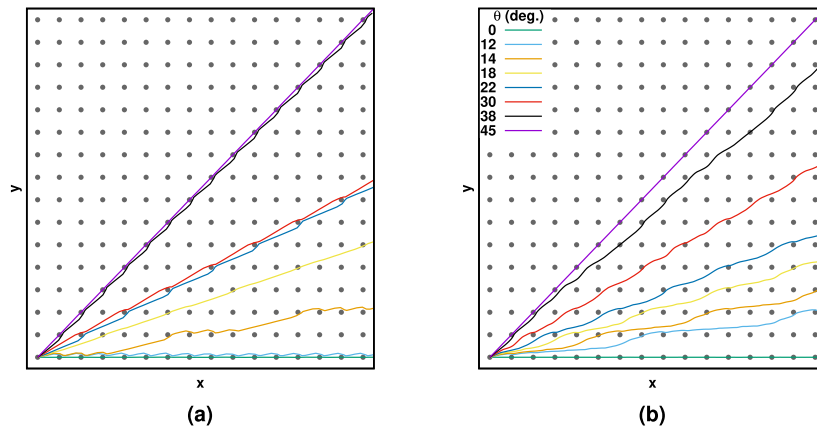


Figure 2. Typical trajectories, (a) for a point-like particles through periodic 2D potential with parameters, $B = 0.3$ and $T = 10^{-4}$, and (b) for a real size particle with parameters $B = 0.7$ and $T = 10^{-4}$.

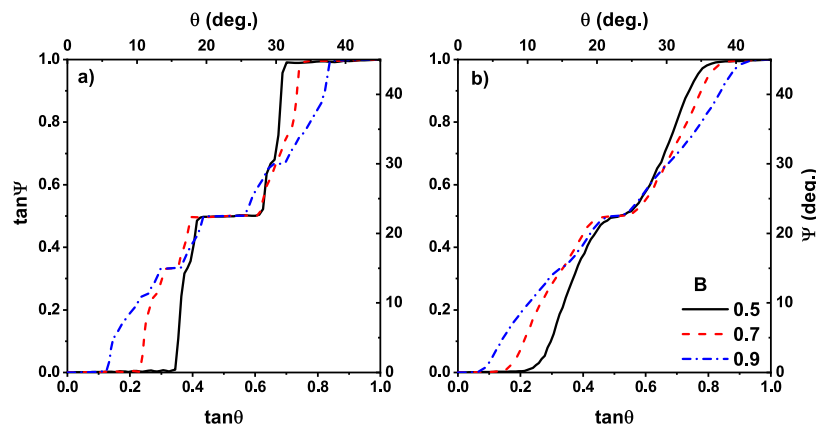


Figure 3. Absolute velocity angle vs. external force direction. Plateaus are observed in the absolute velocity angle for a point-like particle, for different values of control parameter B . Data in (a,b), respectively, correspond to dimensionless temperature $T = 10^{-4}$ and $T = 10^{-2}$. Solid black line, dashed red line and dotted blue line, respectively, correspond to the control parameter $B = 0.5, 0.7$ and 0.9 . Graphs are similar to the data of Ref.³¹.

we calculate $\langle v_{\parallel} \rangle$ and $\langle v_{\perp} \rangle$, where, respectively, are the parallel and perpendicular velocity components relative to external force \mathbf{f} using the following transformations:

$$\begin{aligned} \langle v_{\parallel} \rangle &= \langle v_x \rangle \cos \theta + \langle v_y \rangle \sin \theta, \\ \langle v_{\perp} \rangle &= -\langle v_x \rangle \sin \theta + \langle v_y \rangle \cos \theta. \end{aligned} \tag{9}$$

Both deflection angle α (which is the angle of trajectory measured with respect to the applied force direction) or absolute velocity angle Ψ were used to explore the deviation,

$$\tan \Psi \equiv \frac{\langle v_y \rangle}{\langle v_x \rangle}, \text{ and } \tan \alpha \equiv \frac{\langle v_{\perp} \rangle}{\langle v_{\parallel} \rangle}, \tag{10}$$

where the absolute angle is $\Psi = \theta + \alpha$ (see Fig. 1c).

Figure 2a,b show the typical trajectories, respectively, for point-like particles and real size particles for applied force directions shown in the figure. The reason for the deviations of particle trajectories from the flow field directions is clearly shown in the figure. The particles are attracted to the traps when they are moving on the surface of the potential landscape and pull away from the force direction and the net angular displacement is observed.

Results and discussion

In order to test our simulator, we first reproduced the results were reported by Lacasta setting a point-like particle where partial trapping does not happen, i. e., a traveling particle is fully trapped or escaped. Results are shown in Fig. 3. This figure is a plot of $\tan \Psi$ as a function of $\tan \theta$ for different control parameter B . Figure 3a belongs to the case when the dimensionless temperature is $T = 10^{-4}$ while it is $T = 10^{-2}$ in Fig. 3b. All other parameters have the same numeric value as the original paper of Lacasta et al.³¹. These figures are similar to those of Lacasta,

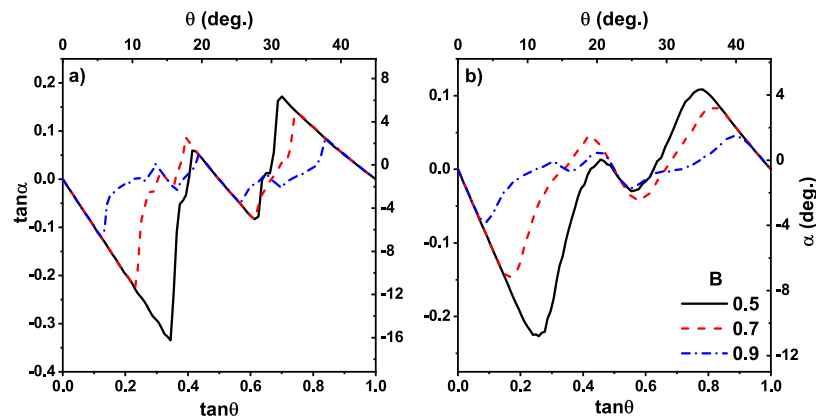


Figure 4. Deflection angle versus external force direction for point-like particle and different control parameter B . (a,b) Correspond to the dimensionless temperature $T = 0.01$ and $T = 0.1$, respectively. Data correspond to control parameter $B = 0.5$ (solid black line), $B = 0.7$ (dashed red line) and $B = 0.9$ (dotted blue line). Our Results are in agreement with the results of Ref.³¹.

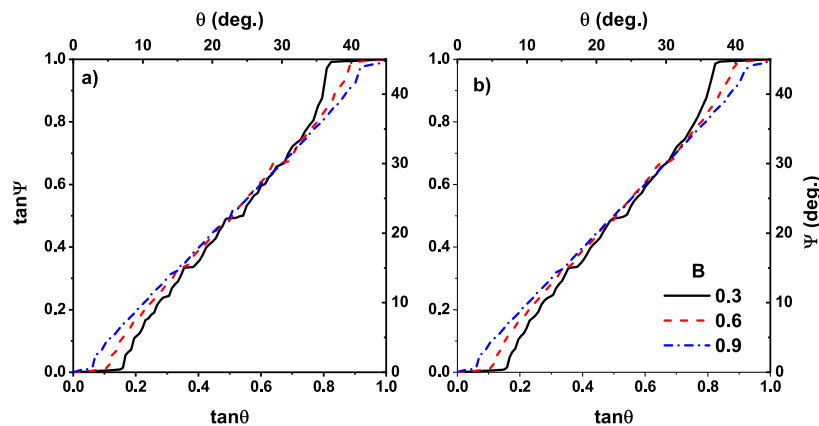


Figure 5. Absolute velocity angle vs. external force direction for real-size particles and different control parameter $B = 0.3$ (solid black line), $B = 0.6$ (dashed red line) and $B = 0.9$ (dotted blue line). (a,b) Correspond to the dimensionless temperature $T = 10^{-4}$ and $T = 10^{-2}$, respectively.

especially in the middle plateau. As it is mentioned earlier, such a large plateau has not seen in any experiment^{1,9}. In addition to the absolute velocity angle, we studied the deflection angle as a function of θ which its results are shown in Fig. 4. Both cases are in good agreement with the results of the point-like particle simulation³¹.

In addition to the simulations done to explain the locked-in phenomenon, some theoretical works are done in the context of probability theory and statistical physics³⁵. In this work, traps are modeled by circles with diameter a which their centers are located at the mesh points of a two-dimensional simple cubic lattice of lattice constant b . Based on the ratio of the $\eta = a/b$, authors defined two distinct regimes: A “ballistic” regime which corresponds to the dilute density of traps (small η) and a regime of packed traps (large η) which are the so called the “lattice gas” regime. Particles in this model is assumed to be point-like too, and as a result, they showed that the plot of $\tan \Psi$ vs $\tan \theta$ has several small plateaus. In order to introduce the effect of thermal fluctuations, they considered that an escaped particle has the freedom to choose its path randomly in an interval of $2\delta\theta$, centered in the flow direction. Introducing the thermal fluctuations caused the calculated results to have better agreement with experiments, however, the size of the middle plateau was much bigger than the experimental results.

Both simulation and theoretical results show that, to have more accurate results with a better agreement with experiment, we need to consider more details in modeling the sorting phenomenon. Ignoring the size of particles and considering them as point-like particles may miss some important details of the system out. To investigate the effect of the particle size on the sorting effect, we set the 16 point-like particles on the circumference of a circle with the diameter $D = 0.4$ in dimensionless scale. In this case, *partial trapping* could happen, i. e., a particle could deviate from its path by the optical tweezers if a fraction of that is illuminated by the focused laser beam.

The results of the simulations are plotted in Figs. 5 and 6. In Fig. 5, we have plotted the absolute velocity angle Ψ as a function of θ for real-size particles. Figure 5a belongs to the dimensionless temperature of $T = 10^{-4}$ and the Fig. 5b is for $T = 10^{-2}$. When $B = 0.3$, which belongs to the wide potential wells (traps), the resulting

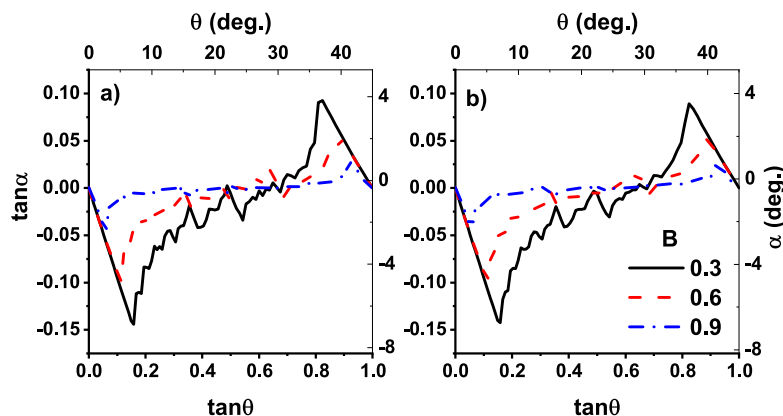


Figure 6. Deflection angle vs field direction for real-size particle for different control parameters $B = 0.3$ (solid black line), $B = 0.6$ (dashed red line) and $B = 0.9$ (dotted blue line). (a,b) Correspond, respectively, to the dimensionless temperatures $T = 10^{-4}$, and $T = 10^{-2}$.

curve has a good agreement with those of experimental observation¹, size of their middle plateaus decreases in both Fig. 5a,b. This is true for thinner potential wells corresponding to the control parameter $B = 0.6$ and 0.9 too. In contrast, the size of first ($\tan \theta < 0.2$) and last ($\tan \theta > 0.8$) plateaus depends on B . This is due to the existence of a wider cross-section of collision in the case of a wider trap. Furthermore, as it is observed in the experiment¹, particles are locked in the directions of $[10]$ ($\tan \Psi = 0$) and $[1\bar{1}]$ ($\tan \Psi = 1$) when $\tan \theta < 0.2$ and $\tan \theta > 0.8$ respectively, therefore, a wider cross-section of collisions results in larger plateaus. Besides, transitions between plateaus occur in the $\tan \theta = 0.3, 0.5, 0.6$, in agreement with experiment¹. Directional locking observed in the experiments of separation of particles using periodic obstacles too^{14,15,18,20,21}. In the paper by Devendra et al.¹⁵, the locking phenomenon takes place in the migration angle $\Psi \approx 0^\circ, 20^\circ, 27^\circ, 45^\circ$ for different particle sizes driven with gravity. Risbud *et al* showed that particles moving through a lattice of obstacles lock-in $\tan \Psi \approx 0, 0.2, 0.3, 0.5, 0.7, 1$ directions¹⁸, which is consistent with the results of our simulation. In the obstacle case directional locking observes when the particles are trapped in the channels between obstacles, while for periodic potential landscape, hopping particle between adjacent traps is the main mechanism of path locking. In latter case, however, traps make a channel in direction $[10]$ and $[1\bar{1}]$ which its width depends on B , as schematically represented in Fig. 1c. These trapping channels are the main reason for existence relatively large plateaus for $\theta < 0.2$ and $\theta > 0.8$, particles entering the lattice in these angles, have less chance to leave the channel. This can be obtained from Fig. 6 too, where the deflection angle α is more pronounced for $\tan \theta < 0.2$ and $\tan \theta > 0.8$.

Figure 5 indicates the fact that temperature has not any significant effect on the size of the middle plateau. The curves become just smoother by increasing T . Indeed there is a competition between thermal fluctuations as the random force and forces imposed by optical traps. Depending on the depth of the potential well, if enough time is given to a trapped particle, thermal fluctuations provide it an opportunity to escape. By increasing temperature, thermal fluctuations strengthen or equivalently, traps become weaker. This is clear from the dimensionless form on temperature $\hat{T} \sim T/V_0$. Therefore particles have less bound to the potential wells in higher temperatures, resulting in smoother curves. Furthermore, the initial and final plateaus have a small deviation from their values at zero temperature (compare with the results of theoretical work³⁵) which indicating again on the fact that our results are not sensitive to the temperature and the increasing two orders of magnitude in temperature is negligible. In addition to the middle plateau, the size of the other plateaus become more realistic in our model, especially ones that correspond to the $\theta > \tan^{-1}(0.8)$. In contrast with point-like particle simulations, our results are more similar to the experiments. Effect of temperature also appears in Fig. 6, were increasing the temperature resulted in smoother graphs.

Increasing the numeric values of the parameter B causes a decrease in the width of traps. Thinner trap, weaker locked-in effect and consequently, smaller plateaus appear. On the other hand, as it is shown in both Figs. 3 and 5, by increasing B size of all plateaus decrease. This is another evidence that the numeric value of B is not a good choice for controlling the particle size, the particle's geometry should be included explicitly in any physical simulation.

Conclusions

In summary, we modeled a real-size particle with a combination of point-like particles on the circumference of a circle which are connected with the same springs. By solving the Langevin equation under the influence of constant external field and thermal fluctuations, we studied the transport of colloidal particles on a two-dimensional surface with periodic potential wells. This model explains those features have been observed in the experimental investigations. It was shown that the partial trapping of the particles which occurs in the array of potential wells could explain the difference between experimental and simulation results. Besides, we showed that the temperature has a negligible effect on the appearance of plateaus.

We showed that by considering the size of particles explicitly in our model, the large middle plateau which appeared in previous simulations becomes smaller and has a better agreement with experimental results. In addition we showed that plateaus corresponding to $\tan \theta > 0.8$ and $\tan \theta < 0.2$ fit well with experiments.

Our work can be extended in some directions. We assumed quasi-spherical rigid particles for our simulations but this method can be used to simulate particles with more complex geometries such as elliptical shape rings. Furthermore, particles with less rigidity can be simulated with this model too, says deformable half side particles. Our model also can be extended to simulate the directional locking and sorting of Janus particles. The flexible particles called skyrmions²⁷ are of current interest, thus, the model can be used to simulate the sorting of them.

Received: 21 December 2019; Accepted: 8 September 2020

Published online: 26 October 2020

References

- Korda, P. T., Taylor, M. B. & Grier, D. G. Kinetically locked-in colloidal transport in an array of optical tweezers. *Phys. Rev. Lett.* **89**, 128301. <https://doi.org/10.1103/PhysRevLett.89.128301> (2002).
- MacDonald, M. P., Spalding, G. C. & Dholakia, K. Microfluidic sorting in an optical lattice. *Nature* **426**, 421–424. <https://doi.org/10.1038/nature02144> (2003).
- Wang, M. M. *et al.* Microfluidic sorting of mammalian cells by optical force switching. *Nat. Biotechnol.* **23**, 83–87. <https://doi.org/10.1038/nbt1050> (2005).
- Dholakia, K. *et al.* Optical separation of cells on potential energy landscapes: enhancement with dielectric tagging. *IEEE J. Select. Top. Quantum Electron.* **13**, 1646–1654. <https://doi.org/10.1109/JSTQE.2007.911314> (2007).
- Dholakia, K., MacDonald, M. P., Zemánek, P. & Čížmár, T. Cellular and colloidal separation using optical forces. *Methods Cell Biol.* **82**, 467–495 (2007).
- Xiao, K. & Grier, D. G. Sorting colloidal particles into multiple channels with optical forces: prismatic optical fractionation. *Phys. Rev. E* **82**, 051407 (2010).
- Herrmann, J., Karweit, M. & Drazer, G. Separation of suspended particles in microfluidic systems by directional locking in periodic fields. *Phys. Rev. E* **79**, 061404 (2009).
- Speer, D., Eichhorn, R. & Reimann, P. Exploiting lattice potentials for sorting chiral particles. *Phys. Rev. Lett.* **105**, 090602 (2010).
- Bohlein, T. & Bechinger, C. Experimental observation of directional locking and dynamical ordering of colloidal monolayers driven across quasiperiodic substrates. *Phys. Rev. Lett.* **109**, 058301 (2012).
- Ma, B. *et al.* Optical sorting of particles by dual-channel line optical tweezers. *J. Opt.* **14**, 105702 (2012).
- Chen, K.-Y., Lee, A.-T., Hung, C.-C., Huang, J.-S. & Yang, Y.-T. Transport and trapping in two-dimensional nanoscale plasmonic optical lattice. *Nano Lett.* **13**, 4118–4122 (2013).
- Huang, L. R., Cox, E. C., Austin, R. H. & Sturm, J. C. Continuous particle separation through deterministic lateral displacement. *Science* **304**, 987–990 (2004).
- Koplik, J. & Drazer, G. Nanoscale simulations of directional locking. *Phys. Fluids* **22**, 052005 (2010).
- Bowman, T., Frechette, J. & Drazer, G. Force driven separation of drops by deterministic lateral displacement. *Lab Chip* **12**, 2903–2908 (2012).
- Devendra, R. & Drazer, G. Gravity driven deterministic lateral displacement for particle separation in microfluidic devices. *Anal. Chem.* **84**, 10621–10627 (2012).
- Bernate, J. A., Liu, C., Lagae, L., Konstantopoulos, K. & Drazer, G. Vector separation of particles and cells using an array of slanted open cavities. *Lab Chip* **13**, 1086–1092 (2013).
- Ye, S., Shao, X., Yu, Z. & Yu, W. Effects of the particle deformability on the critical separation diameter in the deterministic lateral displacement device. *J. Fluid Mech.* **743**, 60–74 (2014).
- Risbud, S. R. & Drazer, G. Directional locking in deterministic lateral-displacement microfluidic separation systems. *Phys. Rev. E* **90**, 012302 (2014).
- Risbud, S. R. & Drazer, G. Mechanism governing separation in microfluidic pinched flow fractionation devices. *Microfluid. Nanofluid.* **17**, 1003–1009 (2014).
- Hanasoge, S., Devendra, R., Diez, F. J. & Drazer, G. Electrokinetically driven deterministic lateral displacement for particle separation in microfluidic devices. *Microfluid. Nanofluid.* **18**, 1195–1200 (2015).
- Du, S., Shojaei-Zadeh, S. & Drazer, G. Liquid-based stationary phase for deterministic lateral displacement separation in microfluidics. *Soft Matter* **13**, 7649–7656 (2017).
- Chen, K. *et al.* Colloidal transport within nematic liquid crystals with arrays of obstacles. *Soft Matter* **14**, 83–91 (2018).
- Salafi, T., Zhang, Y. & Zhang, Y. A review on deterministic lateral displacement for particle separation and detection. *Nano-Micro Lett.* **11**, 77 (2019).
- Grier, D. G. A revolution in optical manipulation. *Nature* **424**, 810–816. <https://doi.org/10.1038/nature01935> (2003).
- Nguyen, H., Reichhardt, C. & Reichhardt, C. O. Clogging and jamming transitions in periodic obstacle arrays. *Phys. Rev. E* **95**, 030902 (2017).
- Tahir, M. A., Gao, L., Virgin, L. N. & Yellen, B. B. Transport of superparamagnetic beads through a two-dimensional potential energy landscape. *Phys. Rev. E* **84**, 011403 (2011).
- Reichhardt, C., Ray, D. & Reichhardt, C. O. Quantized transport for a skyrmion moving on a two-dimensional periodic substrate. *Phys. Rev. B* **91**, 104426 (2015).
- Reichhardt, C. & Nori, F. Phase locking, devil's staircases, farey trees, and arnold tongues in driven vortex lattices with periodic pinning. *Phys. Rev. Lett.* **82**, 414 (1999).
- Reichhardt, C. & Reichhardt, C. O. Structural transitions and dynamical regimes for directional locking of vortices and colloids driven over periodic substrates. *J. Phys.* **24**, 225702 (2012).
- Stoop, R. L., Straube, A. V., Johansen, T. H. & Tierno, P. Collective directional locking of colloidal monolayers on a periodic substrate. *Phys. Rev. Lett.* **124**, 058002 (2020).
- Lacasta, A. M., Sancho, J. M., Romero, A. H. & Lindenberg, K. Sorting on periodic surfaces. *Phys. Rev. Lett.* **94**, 160601. <https://doi.org/10.1103/PhysRevLett.94.160601> (2005).
- Ramachandran, P. & Varoquaux, G. Mayavi: 3D visualization of scientific data. *Comput. Sci. Eng.* **13**, 40–51 (2011).
- Honeycutt, R. L. Stochastic runge-kutta algorithms. I. White noise. *Phys. Rev. A* **45**, 600–603. <https://doi.org/10.1103/PhysRevA.45.600> (1992).
- Press, W. H., Teukolsky, S. A., Vetterling, W. T. & Flannery, B. P. *Numerical Recipes 3rd Edition: The Art of Scientific Computing* (Cambridge University Press, 2007), 3 edn.
- Gopinathan, A. & Grier, D. G. Statistically locked-in transport through periodic potential landscapes. *Phys. Rev. Lett.* **92**, 130602. <https://doi.org/10.1103/PhysRevLett.92.130602> (2004).

Acknowledgements

E. N. O. thanks Dr S. N. S. Reihani for his useful discussions.

Author contributions

This work idea is given by SE.N.O, and, the code was developed by SE.N.O and M.B. The simulations are conducted by M.B., E.M wrote the manuscript and prepared the results. F.M. had contributions in the preparation of the manuscript revisions. All authors reviewed the manuscript.

Competing interests

The authors declare no competing interests.

Additional information

Correspondence and requests for materials should be addressed to S.N.O.

Reprints and permissions information is available at www.nature.com/reprints.

Publisher's note Springer Nature remains neutral with regard to jurisdictional claims in published maps and institutional affiliations.



Open Access This article is licensed under a Creative Commons Attribution 4.0 International License, which permits use, sharing, adaptation, distribution and reproduction in any medium or format, as long as you give appropriate credit to the original author(s) and the source, provide a link to the Creative Commons licence, and indicate if changes were made. The images or other third party material in this article are included in the article's Creative Commons licence, unless indicated otherwise in a credit line to the material. If material is not included in the article's Creative Commons licence and your intended use is not permitted by statutory regulation or exceeds the permitted use, you will need to obtain permission directly from the copyright holder. To view a copy of this licence, visit <http://creativecommons.org/licenses/by/4.0/>.

© The Author(s) 2020